Modelling and Simulation of Heat Transfer through the Finned Hollow Cylindrical Surfaces of an Insulation Testing Rig

Article *in* World Journal of Modelling and Simulation · January 2019

CITATIONS
2

READS
657

5 authors, including:

Stephen Ndubuisi Nnamchi
Kampala International University (KIU)
39 PUBLICATIONS **127** CITATIONS
SEE PROFILE

Onyinyechi Adanma Nnamchi
Michael Okpara University of Agriculture, Umudike
14 PUBLICATIONS **49** CITATIONS
SEE PROFILE

Martins Onyekwelu Onuorah
Kampala International University (KIU)
23 PUBLICATIONS **113** CITATIONS
SEE PROFILE

Emmanuel O. Sangotayo
Ladoke Akintola University of Technology
29 PUBLICATIONS **17** CITATIONS
SEE PROFILE

ISSN 1 746-7233, England, UK
World Journal of Modelling and Simulation
Vol. 15 (2019) No. 3, pp. 243-261

Modelling and Simulation of Heat Transfer through the Finned Hollow Cylindrical Surfaces of an Insulation Testing Rig

Stephen Ndubuisi Nnamchi[1*], Onyinyechi Adanma Nnamchi[2], Martins Onyekwelu Onuorah[3], Emmanuel Olayimika Sangotayo[1], Vincent Gabriel[4]

[1] Department of Mechanical Engineering, SEAS, Kampala International University, Ggaba Road, Kansanga, P.O.B 20000 Kampala, Uganda,
[2] Department of Agricultural Engineering and Bio Resources, Michael Okpara University of Agriculture, Umudike, Umuahia, Nigeria
[3] Department of Physical Sciences, Kampala International University, Ggaba Road, Kansanga, P.O.B 20000 Kampala, Uganda
[4] Department of Electrical/Telecommunication/Computer Engineering, SEAS, Kampala International University (KIU), P.O.B 20000 Ggaba Road, Kansanga, Kampala, Uganda

(*Received March 12 2019, Accepted June 14 2019*)

Abstract. Modelling of heat transfer through the finned hollow cylindrical surfaces of an insulation testing rig (ITR) is the main concern of this work. A differential volume approach was employed in developing thermal differential models. The analytical solutions of the emerging models were sought to establish the actual mathematical functions governing the thermal behaviour of the cylindrical surfaces of the ITR. Moreover, modelling and simulation was accompanied by experimentation. The mathematical functions describing the behaviour of the ITR were made-up of Euler exponential and linear functions. The simulated results validated well with the distributed experimental data. Besides, the thermophysical properties; fin parameter (12/m), thermal conductivity (51.929 W/mK) and thermal diffusivity (0.0000036883 m^2/s) of the mild steel cylindrical surfaces were established from the analysis which in good agreement with the literature results (54 W/mK; 0.00000367 m^2/s). Moreover, the thermal distribution coefficients (0.333333 $\sim$ 0.492247) gave rise to the solution of thermal dynamic model which conformed to the experimental results. Hence, the good agreement between the present and literature results supports that analytical technique could be employed in determining the thermophysical properties of materials. Moreover, the present work recommends that the ITR should be employed in verifying the thermophysical properties of several materials.

Keywords: Modelling, model solution, simulation, heat transfer, fin parameter, thermophysical properties, ITR.

1 Introduction

Fundamentally, insulation testing rig is a novel equipment for determining the thermophysical properties of materials via modelling (analysis) and experimentation. The design and fabrication of insulation testing rig has been accomplished by Nnamchi et al. [13]. The three fold design encompasses geometric, stress and thermal designs of the equipment. The sensible behaviour of the insulation testing rig has not been systematically investigated and needs to be accomplished through modelling and simulation of the system (ITR).

Modelling is an art of discovering the mathematical functions which characterize the real behaviour of an engineering system. In accordance Oko [15] opined that modelling is an art of representing nature (real-world) into mathematical terms. Moreover, Eykhoff in [18] defined a mathematical model as "a representation of the

* Corresponding author. *E-mail address*: stephen.nnamchi@kiu.ac.ug

essential aspects of an existing system (or a system to be constructed) which presents knowledge of that system in usable form".

Precisely, thermal model is a collection of differential equations, which is capable of describing the intricate behaviour of a typical engineering system [11]. Integration of the differential equations gives a closed model solution, which is a combination or assemblage of different mathematical functions capable of predicting the behaviour of an engineering system satisfactorily. Primarily, thermal models are formulated by application of energy conservation principles on a differential or elemental volume of an engineering system. Explicitly, the governing assumptions for simplifying the differential model have to be stated. According to White [23] too many assumptions make the model solution or simulated results to appreciably deviate from the experimental results. Thus, a good model should be developed on minimal assumption for there to be a strong agreement between the empirical and simulated results. Consequently, a minimal assumption will be considered in modelling heat transfer through the insulation testing rig (ITR) sequel to difficulty in measuring the mid-fluid temperature between the two cylindrical surfaces. Systematically, the mid-fluid temperature will be based on individual contribution of the inner and outer heat transfer fluid temperatures.

Conventionally, the analytical (exact or closed) solution is ideal for less complex engineering systems like the ITR whereas the numerical solution is appropriate for more complex engineering systems. For the purposes of precision and proof of new ideas, the analytical solution is preferred to numerical or approximate solution. However, Creosteanu et al [3] is of view that equal accuracy is attained with a much smaller step size of numerical iterations, which may culminate in good agreement between the analytical and numerical results. Nevertheless, the present work is of opinion that analytical solution should be given priority in solving the developed differential equations. In accordance, the current work will strive to provide analytical or closed solutions to the emerging initial value problem (IVP), boundary value problem (BVP) and distributed problem (IBVP) upon superposition of IVP and BVP.

Pertinently, the specific solution is to be obtained by careful description of the initial condition and boundary conditions such as Dirichlet (first kind boundary condition), Neumann (second kind boundary condition) and Newton (third kind boundary condition) which represent the potential, flux and mixture of potential and flux, respectively [2]. The specific model solution will be useful for simulation, which has an added advantage of presenting a detailed information about the engineering system being considered. However, experimentation is necessary for the validation of simulated results from the model solution [22]. Hence, modelling and simulation cannot standalone; it must be accompanied by measurement (experimentation). In compliance, the present work will present both experimental and simulated data for the holistic analysis of the ITR.

Consequently, the important thermal properties of the system (ITR) could be derived from the post processing of the experimental and simulated data. Therefore, the present work is expected to unveil or derive the thermal conductivity from the fin parameter and thermal diffusivity of the bare cylindrical test surface of the ITR or that of an overlaid insulating material on the ITR from the time additive solution of the thermal model. Moreover, the benefit of modelling and simulation of an engineering systems goes beyond the art of discovering the physical properties of the system; it furnishes information which are difficult to access by measurement as a result of restriction on the system configuration. Similar challenge will be encountered in the ITR in measuring the mid-fluid temperature between the concentric cylindrical test surfaces. Besides, modelling and simulation of ITR offers an analytical technique for determining the thermal conductivity and diffusivity of materials which does not require sophisticated equipment nor special test condition compared to other test techniques or equipment like heat flow meter [5], guarded heat flow meters [19], guarded hot plate instrument [10], flash diffusivity methods [12], calibrated hot box [9], and inverse problem method [8].

Thus, the present work is aimed at; developing mechanistic or differential thermal models capable of describing the behaviour of the ITR, solving the emerging differential models, validating the model solution and deducing the thermophysical properties of the mild steel surface or an overlaid material(s). The rest of the synopsis is; materials and method with experimentation and model formulation inclusively; the detailed discussion of the results; conclusion on the detailed results; and the references.

2 Materials and method

The proposed state of the art requires availability of the following materials: an insulation testing rig (ITR), digital multimeters (thermocouples), vernier caliper, measuring tape, stop watch, electrical heater, marker and rubber clips for the experimentation; formulation of mathematical model and simulation of the thermal fluxes (conductive and convective) around the cylindrical surface of the ITR.

2.1 Experimentation

The cylindrical surface of the ITR was fitted with five UNI-T (UT33C+) and one Allsun (EM420A) digital multimeters (thermocouples) to measure the spatial temperature distribution along the cylindrical surface, while the seventh thermocouple, UNI-T (UT33C+) was permanently inserted into the finned bath for measuring temperature of the interior working fluid (air), whereas the eighth and last multimeter UNI-T (UT33C+ thermocouple) was used to measure the temperature of an external working fluid (air). A stainless vernier caliper (TOKYO) was used to gauge the diameter of the cylindrical surfaces. The measuring tape (AMS56 50m Tape measure) and marker (MK-MP10) was used to calibrate temperature measuring points. The tips of the multimeter were fastened on the cylindrical surface with the aid of the rubber clips. The experimental data were logged while cooling the heated ITR. Temperature was recorded on two minutes interval until a steady state condition was almost attained at 2.34 hours ($\approx$ 2:20:30). The experimental setup is pictorially represented in Fig. 1.

Fig. 1: Insulation testing rig with a projected cylindrical test surface.

2.2 Model formulation

Considering energy balance around the concentric cylindrical differential volume in Fig. 2 and Fig. 3; component energy balance equation or uncoupled thermal model will be developed. The component balance constitutes energy balance on the outer (o) and inner (i) cylinders.

Analytically, the thermal potential is varying in space (x-axis) and time; it is well-known as the excess temperature between the cylindrical surface and fluid surrounding them.

The thermal fluxes consist of conductive thermal flux (Q_x) which flows in the direction perpendicular to the cross sectional area whereas the convective flux (dQ) flows perpendicular to the curved surface or perimeter of the cylinders.

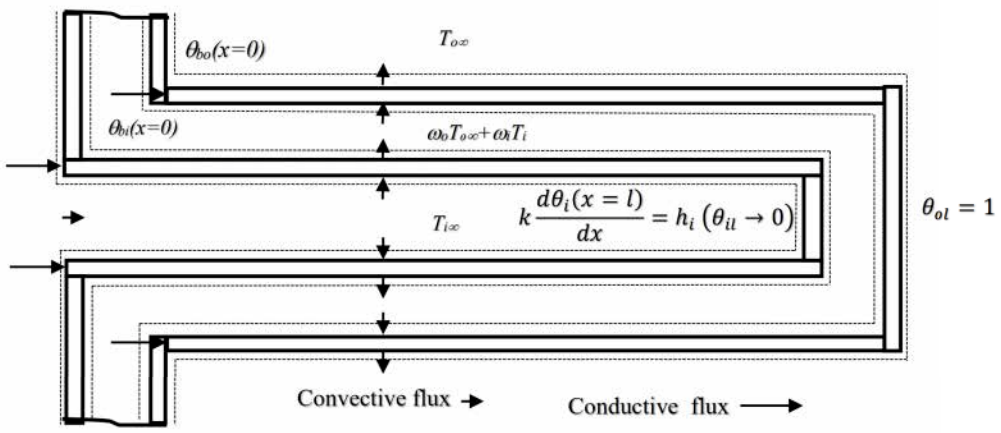

Fig. 2: Vectorial representation of heat flux on the cylindrical surface of an insulation testing rig.

The thermal transport between the two cylindrical bodies results in uncoupled heat transfer equations. The unsteady state excess temperature balance along the cylindrical surface is expressed in Eq. (2) as follows:

Energy accumulation within the cylindrical surface = energy input across the cylindrical surface - energy output across the cylindrical surface. (1)

Thermal balance at the outer cylinder is given in Eqs. (2) and (2) as

$$A_{co}\rho\,\mathrm{cp}\,\frac{\partial\theta_o}{\partial t} = kA_{co}\frac{\partial^2\theta_o}{\partial x^2} - h_{oo}P_{oo}\theta_o + h_{oi}P_{oi}\left[\left(\omega_i T_{i\infty} + (\omega_o - 1)\,T_{o\infty}\right) - \theta_o\right] \tag{2}$$

where

$$\theta_o = T_{so} - T_{o\infty}; \quad \left(\omega_i T_{i\infty} + (\omega_o - 1)\,T_{o\infty}\right) - \theta_o = \omega_i T_{i\infty} + \omega_o T_{o\infty} - T_{so} \tag{3}$$

where $A_{co}(m^2)$is the cross sectional area of the outer cylinderical surface available to the conductive thermal flux, $\theta_o(K)$ is the excess temperature along the outer cylindrical surface, (kg/m^3) is the density of the cylindrical surface, $cp(kJ/kgK)$ is the heat capacity of the cylindrical surface, $t(s)$ is the time required for the heat transfer, $k(W/mK)$ is the thermal conductivity of the cylindrical surface, $x(m)$ is the dimension in x-axis, $h_{oo}(W/m^2K)$ is the convective heat transfer coefficient between the outer cylinder and ambient, $h_{oi}(W/m^2K)$ is the convective heat transfer coefficient between the outer cylinder and mid-fluid, $T_{o\infty}(K)$ is the ambient temperature, $T_{i\infty}(K)$ is the fluid temperature within the inner cylindrical surfaces, $P_{oo}(m)$ is the perimeter of the outer surface of outer cylinder available to convective heat flux, $P_{oi}(m)$ is the perimeter of the inner surface of outer cylinder available to convective heat flux, $\omega_i(-)$ and $\omega_o(-)$ is the individual contribution of $T_{i\infty}$ and $T_{o\infty}$, respectively to the mid-fluid temperature, T_{so} is the temperature of the outer cylindrical surface, and T_{si} is the temperature of the inner cylindrical surface.

Similarly, thermal balance around the inner cylinder is expressed in Eqs. (4) and (5) is as follows:

$$A_{ci}\rho\,\mathrm{cp}\,\frac{\partial\theta_i}{\partial t} = kA_{ci}\frac{\partial^2\theta_i}{\partial x^2} - h_{io}P_{io}\theta_i + h_{ii}P_{ii}\left[\left(1-\omega_i\right)T_{i\infty} - \omega_o T_{o\infty} - \theta_i\right] \tag{4}$$

where

$$\theta_i = T_{si} - \left(\omega_i T_{i\infty} + \omega_0 T_{0\infty}\right); \quad \left(1-\omega_i\right)T_{i\infty} - \omega_o T_{o\infty} - \theta_i = T_{i\infty} - T_{si} \tag{5}$$

where $A_{ci}(m^2)$ is the cross sectional area of the inner cylinder available to the conductive thermal flux, $\theta_i(K)$ is the excess temperature along the inner cylindrical surface, $h_{ii}(W/m^2K)$ is the convective heat transfer coefficient below the inner cylinder, $h_{io}(W/m^2K)$ is the convective heat transfer coefficient between the inner cylinder and mid-fluid, $P_{ii}(m)$ is the perimeter of the inner surface of the inner cylinder cylinder available to convective heat flux and $P_{io}(m)$ is the perimeter of the outer surface of the inner cylinder available to convective heat flux.

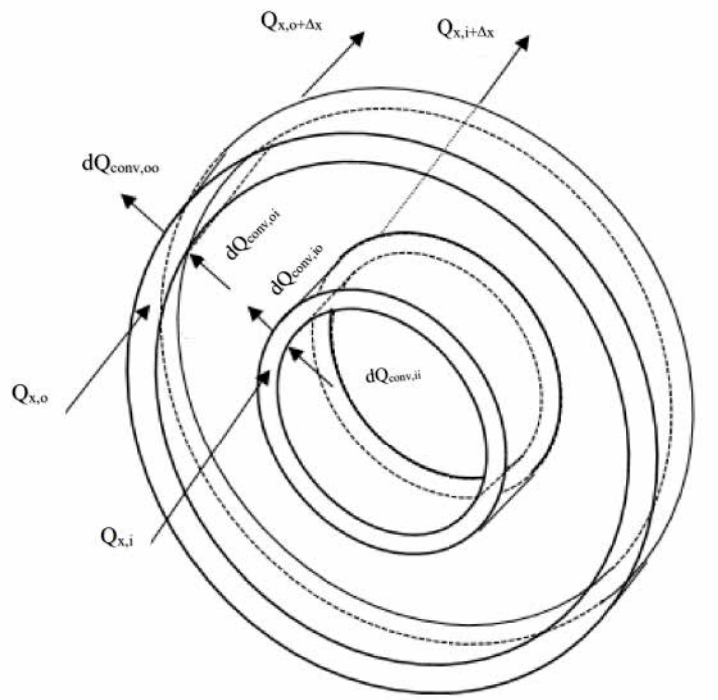

Fig. 3: The differential volume of thermal flux on the cylindrical surfaces

Rearranging Eqs. (2) and (4) yields Eq. (6) for the outer cylindrical surface

$$\frac{\partial\theta_o}{\partial t} = \frac{k}{\rho cp}\frac{\partial^2\theta_o}{\partial x^2} - \frac{h_{oo}P_{oo}}{A_{co}\rho cp}\theta_o + \frac{h_{oi}P_{oi}}{A_{co}\rho cp}\left[\left(\omega_i T_{i\infty} + \left(\omega_o - 1\right)T_{o\infty}\right) - \theta_o\right] \tag{6}$$

and Eq. (7) for the inner cylindrical surface

$$\frac{\partial\theta_i}{\partial t} = \frac{k}{\rho cp}\frac{\partial^2\theta_i}{\partial x^2} - \frac{h_{io}P_{io}}{A_{ci}\rho cp}\theta_i + \frac{h_{ii}P_{ii}}{A_{ci}\rho cp}\left[\left(1-\omega_i\right)T_{i\infty} - \omega_o T_{o\infty} - \theta_i\right] \tag{7}$$

respectively.

The thermal diffusivity, $\alpha(m^2/s)$ of the mild steel cylindrical surface is defined in Eq. (8) as follows:

$$\alpha = \frac{k}{\rho cp} \tag{8}$$

and the unsteady state fin parameter, $n_o^2(1/s)$ for the outer cylindrical surface is given in Eq. (9) as

$$n_o^2 = \frac{h_{oo}P_{oo} + h_{oi}P_{oi}}{A_{co}\rho\,cp}; n_o^* = \frac{h_{oi}P_{oi}}{A_{co}\rho\,cp}\left(\omega_i T_{i\infty} + \left(\omega_o - 1\right)T_{o\infty}\right) \tag{9}$$

and the unsteady state fin parameter, n_i^2 for the inner cylindrical surface is stated in Eq. (10) as follows:

$$n_i^2 = \frac{h_{ii}P_{ii} + h_{io}P_{io}}{A_{ci}\rho\, cp}; n_i^* = \frac{h_{ii}P_{ii}}{A_{ci}\rho\, cp}\left(\left(1-\omega_i\right)T_{i\infty} - \omega_o T_{o\infty}\right) \tag{10}$$

where n_o^* and n_i^* is unsteady state nonlinear heat source term in Eqs. (6) and (7), respectively.

Also, imposing steady state condition to Eqs. (6) and (7) gives Eq. (11)

$$\frac{d^2\theta_o}{dx^2} - \frac{h_{oo}P_{oo}}{A_{co}k}\theta_o + \frac{h_{oi}P_{oi}}{A_{co}k}\left[\left(\omega_i T_{i\infty} + \left(\omega_o - 1\right)T_{o\infty}\right) - \theta_o\right] \tag{11}$$

and Eq. (12)

$$\frac{d^2\theta_i}{dx^2} - \frac{h_{io}P_{io}}{A_{ci}k}\theta_i + \frac{h_{ii}P_{ii}}{A_{ci}k}\left[\left(1-\omega_i\right)T_{i\infty} - \omega_o T_{o\infty} - \theta_i\right] \tag{12}$$

respectively.

Letting

$$m_o^2 = \frac{h_{oo}P_{oo} + h_{oi}P_{oi}}{A_{co}k}; m_o^* = \frac{h_{oi}P_{oi}}{A_{co}k}\left(\omega_i T_{i\infty} + \left(\omega_o - 1\right)T_{o\infty}\right) \tag{13}$$

in Eq. (13) and

$$m_i^2 = \frac{h_{ii}P_{ii} + h_{io}P_{io}}{A_{ci}k}; m_i^* = \frac{h_{ii}P_{ii}}{A_{ci}k}\left(\left(1-\omega_i\right)T_{i\infty} - \omega_o T_{o\infty}\right) \tag{14}$$

in Eq. (14).

where m_o^2 and m_i^2 is fin parameter at steady state condition, m_o^* and m_i^* is nonlinear heat source terms in Eqs. (11) and (12), respectively.

Then, Eq. (11) is rewritten in Eq. (15) as

$$\frac{d^2\theta_o}{dx^2} - m_o^2\theta_o + m_o^* = 0 \tag{15}$$

and Eq. (12) is simplified in Eq. (16) as

$$\frac{d^2\theta_i}{dx^2} - m_i^2\theta_i + m_i^* = 0 \tag{16}$$

Thus, a fin parameter for the steady state condition (m_o^2) is related to the one for unsteady state condition (n_o^2) in Eq. (17) for the outer cylindrical surface as

$$m_o^2 = \frac{n_o^2}{\alpha}; m_o^* = \frac{n_o^*}{\alpha}; \Longrightarrow \alpha = \frac{n_o^2}{m_o^2} = \frac{n_o^*}{m_o^*} \tag{17}$$

and in Eq. (18) for the inner cylindrical surface as

$$m_i^2 = \frac{n_i^2}{\alpha}; m_i^* = \frac{n_i^*}{\alpha}; \Longrightarrow \alpha = \frac{n_i^2}{m_i^2} = \frac{n_i^*}{m_i^*} \tag{18}$$

Solving the boundary value problem (BVP) origninating from Eq. (15) for a complementary (homogeneous) solution and particular (nonhomogeneous) solution by method of undetermined coefficient yields the general solution of Eq. (15) in Eq. (19) as follows:

$$\theta_o\left(x\right) = C_{1o}e^{m_o x} + C_{2o}e^{-m_o x} + \frac{m_o^*}{m_o^2} \tag{19}$$

Similarly, solving the BVP in Eq. (16) for both complementary solution and particular solution by method of undetermined coefficient gives the general solution of Eq. (16) in Eq. (20) as

$$\theta_i\left(x\right) = C_{1i}e^{m_i x} + C_{2i}e^{-m_i x} + \frac{m_i^*}{m_i^2} \tag{20}$$

The specific solution of Eqs. (19) and (20) is obtained by imposing experimentally supported boundary conditions as depicted in Fig. 2 and in Eq. (21) for the outer cylindrical surface

$$\theta_o(x=0)=\theta_{bo0};\theta_o(x=l)=\theta_{ol} \tag{21}$$

and in Eq. (22) for the inner cylindrical surface

$$\theta_i(x=0)=\theta_{bi0};\frac{d\theta_i(x=l)}{dx}=\frac{h_i}{k}\theta_{il} \tag{22}$$

Then, Eq. (19) is defined in Eq. (23) as

$$\begin{aligned}\theta_o(x)&=\frac{\theta_{bo0}+\left(m_o^*/m_o^2\right)\left(e^{m_ol}-1\right)-\theta_{0l}e^{m_ol}}{1-e^{2m_ol}}e^{m_ox}+\frac{\theta_{bo0}+\left(m_o^*/m_o^2\right)\left(e^{-m_ol}-1\right)-\theta_{0l}e^{-m_ol}}{1-e^{-2m_ol}}e^{-m_ox}+\frac{m_o^*}{m_o^2}\\ \Rightarrow\ \theta_o(x)&=\frac{\theta_{bo0}+\left(m_o^*/m_o^2\right)\left(e^{m_ol}-1\right)-\theta_{0l}e^{m_ol}}{1-e^{2m_ol}}e^{m_ox}+\frac{\theta_{bo0}+\left(m_o^*/m_o^2\right)\left(e^{-m_ol}-1\right)-\theta_{0l}e^{-m_ol}}{1-e^{-2m_ol}}e^{-m_ox}\\ &\quad+\frac{h_{oi}P_{oi}\left(\omega_iT_{i\infty}+(\omega_o-1)T_{o\infty}\right)}{h_{oo}P_{oo}+h_{oi}P_{oi}}\end{aligned} \tag{23}$$

whereas Eq. (20) conforms to Eq. (24)

$$\begin{aligned}\theta_i(x)&=C_{1i}e^{m_ix}+C_{2i}e^{-m_ix}+m_i^*/m_i^2\\ \theta_i(x)&=\frac{\left(\theta_{bi0}-m_i^*/m_i^2\right)e^{-m_il}+h_{io}\theta_{il}/m_ik}{\left(e^{m_il}+e^{-m_il}\right)}e^{m_ix}+\frac{\left(\theta_{bi0}-m_i^*/m_i^2\right)e^{m_il}-h_{io}\theta_{il}/m_ik}{\left(e^{m_il}+e^{-m_il}\right)}e^{-m_ix}\\ &\quad+\frac{h_{ii}P_{ii}((1-\omega_i)T_{i\infty}-\omega_oT_{o\infty})}{h_{ii}P_{ii}+h_{io}P_{io}}\end{aligned} \tag{24}$$

Substituting Eqs. (8)-(10) into Eqs. (6) and (7) gives the simplified form of Eqs. (6) and (7) in Eq. (25)

$$\frac{\partial\theta_o}{\partial t}=\alpha\frac{\partial^2\theta_o}{\partial x^2}-n_o^2\theta_o+n_o^*;\Longrightarrow\frac{1}{\alpha}\frac{\partial\theta_o}{\partial t}=\frac{\partial^2\theta_o}{\partial x^2}-m_o^2\theta_o+m_o^* \tag{25}$$

and Eq. (26)

$$\frac{\partial\theta_i}{\partial t}=\alpha\frac{\partial^2\theta_i}{\partial x^2}-n_i^2\theta_i+n_i^*;\Longrightarrow\frac{1}{\alpha}\frac{\partial\theta_i}{\partial t}=\frac{\partial^2\theta_i}{\partial x^2}-m_i^2\theta_i+m_i^* \tag{26}$$

respectively.

The solution of Eqs. (25) and (26) is sought by method of additive separation in Eq. (27) for the outer cylindrical surface

$$\theta_o(x,t)=\varphi_o(t)+\psi_o(x);\frac{\partial\theta_o}{\partial t}=\frac{d\varphi_o}{dt};\frac{\partial\theta_o}{\partial x}=\frac{d\psi_o}{dx};\frac{\partial^2\theta_o}{\partial x^2}=\frac{d^2\psi_o}{dx^2} \tag{27}$$

and Eq. (28) for the inner cylindrical surface

$$\theta_i(x,t)=\varphi_i(t)+\psi_i(x);\frac{\partial\theta_i}{\partial t}=\frac{d\varphi_i}{dt};\frac{\partial\theta_i}{\partial x}=\frac{d\psi_i}{dx};\frac{\partial^2\theta_i}{\partial x^2}=\frac{d^2\psi_i}{dx^2} \tag{28}$$

For the initial conditions in Eq. (29)

$$\theta_o(x,0)=\theta_{bo0};\theta_i(x,0)=\theta_{bi0}\forall\quad 0\le x\le l \tag{29}$$

Substituting Eqs. (27) and (28) into Eqs. (25) and (26), respectively gives separable functions in terms of time and space with the separation constants $\lambda_o^\Gamma,\lambda_i^\Gamma$ in Eq. (30) for the outer mild steel cylindrical surface [6]

$$\begin{aligned}&\frac{1}{\alpha}\frac{d\varphi_o(t)}{dt}+m_o^2\varphi_o(t)-\lambda_o^\Gamma=0;\ \Rightarrow\frac{d\varphi_o(t)}{dt}+\alpha m_o^2\varphi_o(t)-\alpha\lambda_o^\Gamma=0;\frac{d^2\psi_o(x)}{dx^2}-m_o^2\psi_o(x)+m_o^*-\lambda_o^\Gamma=o;\\ &\exists\qquad\Gamma=1,2,\cdots,\infty\quad(\text{arbitrary integer number})\end{aligned} \tag{30}$$

and Eq. (31) for the inner cylindrical surface

$$\begin{matrix}\frac{1}{\alpha}\frac{d\varphi_i(t)}{dt}+m_i^2\varphi_i\left(t\right)-\lambda_i^{\Gamma}=0\,;\;\Rightarrow\frac{d\varphi_i(t)}{dt}+\alpha m_i^2\varphi_i\left(t\right)-\alpha\lambda_i^{\Gamma}=0;\frac{d^2\psi_i(x)}{dx^2}-m_i^2\psi_i\left(x\right)+m_i^*-\lambda_i^{\Gamma}=o;\\ \exists\qquad\Gamma=1,\,2,\,\cdots,\,\infty\quad\text{(arbitrary integer number)}\end{matrix}\tag{31}$$

respectively.

Solving the time dependent function in Eqs. (30) and (31) by method of integrating factor and imposing initial condition yields Eq. (32) for the outer cylindrical surface on cooling basis

$$\varphi_o\left(t\right)=\theta_{bo0}\,e^{-\alpha\,m_o^2t}+\frac{\lambda_o^{\Gamma}}{m_o^2}\left(1-e^{-\alpha\,m_o^2t}\right)\tag{32}$$

and Eq. (33) for the inner cylindrical surface on a cooling basis

$$\varphi_i\left(t\right)=\theta_{bi0}\,e^{-\alpha\,m_i^2t}+\frac{\lambda_i^{\Gamma}}{m_i^2}\left(1-e^{-\alpha\,m_i^2t}\right)\tag{33}$$

respectively.

Also, solving the space dependent function in Eqs. (30) and (31) for both homogeneous and nonhomogeneous solutions and imposing the boundary conditions gives the specific closed solution of Eq. (30) in Eq. (34) as

$$\begin{matrix}\psi_o\left(x\right)=\frac{\theta_{bo0}+\left(\left(m_o^*-\lambda_o^{\Gamma}\right)/m_o^2\right)\left(e^{m_ol}-1\right)-\theta_{0l}e^{m_ol}}{1-e^{2m_ol}}e^{m_ox}\\ +\frac{\theta_{bo0}+\left(\left(m_o^*-\lambda_o^{\Gamma}\right)/m_o^2\right)\left(e^{-m_ol}-1\right)-\theta_{0l}e^{-m_ol}}{1-e^{-2m_ol}}e^{-m_ox}+\frac{m_o^*-\lambda_o^{\Gamma}}{m_o^2}\end{matrix}\tag{34}$$

and that of Eq. (31) is given in Eq. (35) as

$$\begin{matrix}\psi_i\left(x\right)=\frac{\left(\theta_{bi0}-\left(m_i^*-\lambda_i^{\Gamma}\right)/m_i^2\right)e^{-m_il}+h_{io}\theta_{il}/m_ik}{\left(e^{m_il}+e^{-m_il}\right)}e^{m_ix}\\ +\frac{\left(\theta_{bi0}-\left(m_i^*-\lambda_i^{\Gamma}\right)/m_i^2\right)e^{m_il}-h_{io}\theta_{il}/m_ik}{\left(e^{m_il}+e^{-m_il}\right)}e^{-m_ix}\end{matrix}\tag{35}$$

The eigenvalue, $\lambda_{o,k};k=1,2,...,\infty$ in Eqs. (31) and (32) is obtained by transcendental equation [1] for the boundary conditions specified in Fig. 2 is expressed in Eq. (36) as

$$\lambda_{o,k}\tan\left(\lambda_{o,k}l_{oo}\right)=\frac{h_{\,io,bath}}{k_{material}}\tag{36}$$

Similarly, the eigenvalue, $\lambda_{i,k};k=1,2,...,\infty$ in Eqs. (31) and (32) is computed by the transcendental equation [1] for the boundary conditions specified in Fig. 2 is written in Eq. (37) as

$$\lambda_{i,k}\tan\left(\lambda_{i,k}l_{ii}\right)=\frac{h_{\,ii,bath}}{k_{material}}\tag{37}$$

A specific solution to Eq. (25) is proposed to be governed by different contributions from IVP and BVP for the outer cylindrical surface in Eq. (38)

$$\begin{matrix}\theta_o\left(x,t\right)=A_o\varphi_o\left(t\right)+B_o\psi_o\left(x\right)=\\ A_o\left(\begin{matrix}\theta_{bo0}\,e^{-\alpha\,m_o^2t}\\ +\frac{\lambda_o^{\Gamma}}{m_o^2}\left(1-e^{-\alpha\,m_o^2t}\right)\end{matrix}\right)+B_o\left(\begin{matrix}\frac{\theta_{bo0}+\left(\left(m_o^*-\lambda_o^{\Gamma}\right)/m_o^2\right)\left(e^{m_ol}-1\right)-\theta_{0l}e^{m_ol}}{1-e^{2m_ol}}e^{m_ox}\\ +\frac{\theta_{bo0}+\left(\left(m_o^*-\lambda_o^{\Gamma}\right)/m_o^2\right)\left(e^{-m_ol}-1\right)-\theta_{0l}e^{-m_ol}}{1-e^{-2m_ol}}e^{-m_ox}\\ +\frac{m_o^*-\lambda_o^{\Gamma}}{m_o^2}\end{matrix}\right)\end{matrix}\tag{38}$$

and similar solution to Eq. (26) is given in Eq. (39) for the inner cylindrical surface

$$\begin{matrix}\theta_i\left(x,t\right)=A_i\varphi_i\left(t\right)+B_i\,\psi_i\left(x\right)=\\ A_i\left(\begin{matrix}\theta_{boi}\,e^{-\alpha\,m_i^2t}\\ +\frac{\lambda_i^{\Gamma}}{m_i^2}\left(1-e^{-\alpha\,m_i^2t}\right)\end{matrix}\right)+B_i\left(\begin{matrix}\frac{\left(\theta_{bi0}-\left(m_i^*-\lambda_i^{\Gamma}\right)/m_i^2\right)e^{-m_il}+h_{io}\theta_{il}/m_ik}{\left(e^{m_il}+e^{-m_il}\right)}e^{m_ix}\\ +\frac{\left(\theta_{bi0}-\left(m_i^*-\lambda_i^{\Gamma}\right)/m_i^2\right)e^{m_il}-h_{io}\theta_{il}/m_ik}{\left(e^{m_il}+e^{-m_il}\right)}e^{-m_ix}\\ +\frac{m_i^*-\lambda_i^{\Gamma}}{m_i^2}\end{matrix}\right)\end{matrix}\tag{39}$$

where A_o and B_o are thermal distribution coefficients of IVP and BVP in Eq. (40), respectively. The thermal distribution coefficients A_o and B_o in Eq. (40) are established by the principal condition; $\theta_o(0,0) = \theta_{bo0}$

$$\theta_o(0,0) = A_o\varphi_{o0} + B_o\psi_{o0} = \theta_{bo0} \tag{40}$$

and minor conditions; $\theta_o(0,\infty) = 0; \theta_o(l,0) = 0$ and $\theta_o(l,\infty) = 0$ in Eq. (41) as follows:

$$\theta_o(0,\infty) = A_o\varphi_{o\infty} + B_o\psi_{o0} = 0; \theta_o(l,0) = A_o\varphi_{o0} + B_o\psi_{ol} = 0; \theta_o(l,\infty) = A_o\varphi_{o\infty} + B_o\psi_{ol} = 0 \tag{41}$$

Combining Eqs. (40) and (41) yields the thermal distribution coefficient A_o in Eq. (42)

$$A_o = \frac{\theta_{bo0}\psi_{o0}}{(\varphi_{o0} - 2\varphi_{o\infty})\left(\psi_{o0} + \frac{\psi_{o0}\varphi_{o0}}{\varphi_{o0} - 2\varphi_{o\infty}}\right)} \tag{42}$$

and B_o in Eqs. (43)

$$B_o = \frac{\theta_{bo0}}{\left(\psi_{o0} + \frac{\psi_{o0}\varphi_{o0}}{\varphi_{o0} - 2\varphi_{o\infty}}\right)} \tag{43}$$

Remarkably, $\varphi_{o\infty} = 0, \Rightarrow A_o = B_o = 0.5$ thus, there is existence of a true solution, $\theta_o(x,t)\, \exists A_o = B_o \leq 0.5$. Similarly, A_i and B_i could be established by the same technique.

2.2.1 Parameter estimation

The perimeter of the inner and outer surfaces of the out cylinder in Eq. (44) is defined as follows:

$$P_{oo} = \pi D_{oo}; P_{oi} = \pi D_{oi} \tag{44}$$

whereas the perimeter of the inner and outer surfaces of the inner cylinder in Eq. (45) is well-defined as

$$P_{ii} = \pi D_{ii}; P_{io} = \pi D_{io} \tag{45}$$

The cross sectional area available for conduction at the outer cylinder is given in Eq. (46) as

$$A_{co} = \frac{\pi}{4}\left(D_{oo}^2 - D_{oi}^2\right) \tag{46}$$

The cross sectional area available for conduction at the inner cylinder is written in Eq. (47) as

$$A_{ci} = \frac{\pi}{4}\left(D_{io}^2 - D_{ii}^2\right) \tag{47}$$

where D is the diameter of the cylindrical geometry.

According to Nnamchi et al. [13] and Nnamchi et al. [14] the external heat transfer coefficient at the outer cylinder is expressed in Eq. (48) as

$$h_{oo} = \frac{k_{air}}{D_{oo}}\left(0.193\,\mathrm{Re}_{D_{oo}}^{0.618}\,\mathrm{Pr}^{1/3}\right) \exists \quad \mathrm{Pr} \geq 0.70,\ 4000 \leq D_{oo} \leq 40000 \tag{48}$$

whereas the internal heat transfer coefficient on the horizontal surface [20, 21] is stated in Eqs. (49)-(51) as follows:

$$\begin{aligned} h_{oi} &\approx \frac{k_{air}}{D_{oi}}\left\{0.60 + \frac{0.387Ra_{D_{oi}}^{1/6}}{\left[1+(0.559/\mathrm{Pr})^{9/16}\right]^{8/27}}\right\}^2 \quad for\ \ 10^{-1} < Ra_{D_{oi}} < 10^{12}, \\ Ra_{D_{oi}} &= Gr_{D_{oi}}\,\mathrm{Pr};\quad Gr_{D_{oi}} = \frac{g\,(D_{oi})^3\beta\,[(\omega_i T_{ii} + \omega_o T_{oo}) - T_{so}]}{\mu^2/\rho^2},\quad \mathrm{Pr} = \frac{\mu_{air}\,cp_{air}}{k_{ar}} \end{aligned} \tag{49}$$

and

$$\begin{aligned} h_{io} &\approx \frac{k_{air}}{D_{io}}\left\{0.60 + \frac{0.387Ra_{D_{io}}^{1/6}}{\left[1+(0.559/\mathrm{Pr})^{9/16}\right]^{8/27}}\right\}^2 \quad for\ \ 10^{-1} < Ra_{D_{io}} < 10^{12}, \\ Ra_{D_{io}} &= Gr_{D_{io}}\,\mathrm{Pr};\quad Gr_{D_{io}} = \frac{g\,(D_{io})^3\beta\,[T_{si} - (\omega_i T_{ii} + \omega_o T_{oo})]}{\mu^2/\rho^2},\quad \mathrm{Pr} = \frac{\mu_{air}\,cp_{air}}{k_{air}} \end{aligned} \tag{50}$$

and

$$h_{ii} \approx \frac{k_{air}}{D_{ii}}\left\{0.60 + \frac{0.387Ra_{D_{ii}}^{1/6}}{\left[1+(0.559/\mathrm{Pr})^{9/16}\right]^{8/27}}\right\}^2 \quad for \quad 10^{-1} < Ra_{D_{ii}} < 10^{12},$$
$$Ra_{D_{ii}} = Gr_{D_{ii}}\,\mathrm{Pr}; \quad Gr_{D_{ii}} = \frac{g\,(D_{ii})^3\beta\,(T_{si}-T_{i\infty})}{\mu^2/\rho^2}, \quad \mathrm{Pr} = \frac{\mu_{air}\,cp_{air}}{k_{air}} \tag{51}$$

Also, the convecctive heat transfer coefficient in the bath is given in Eqs. (52) and (53) [14] as

$$h_{ii,bath} \approx \frac{k_{air}}{l_{ii}}\left\{0.825 + \frac{0.387Ra_{l_{ii}}^{1/6}}{\left[1+(0.492/\mathrm{Pr})^{9/16}\right]^{8/27}}\right\}^2 \quad for \quad 10^{-1} < Ra_{l_{ii}} < 10^{12},$$
$$Ra_{l_{ii}} = Gr_{l_{ii}}\,\mathrm{Pr}; \quad Gr_{l_{ii}} = \frac{g\,(l_{ii})^3\beta\,(T_{i\infty}-T_{si})}{\mu^2/\rho^2}, \quad \mathrm{Pr} = \frac{\mu_{air}\,cp_{air}}{k_{air}} \tag{52}$$

and

$$h_{io,bath} \approx \frac{k_{air}}{l_{io}}\left\{0.825 + \frac{0.387Ra_{l_{io}}^{1/6}}{\left[1+(0.492/\mathrm{Pr})^{9/16}\right]^{8/27}}\right\}^2 \quad for \quad 10^{-1} < Ra_{l_{io}} < 10^{12},$$
$$Ra_{l_{io}} = Gr_{l_{io}}\,\mathrm{Pr}; \quad Gr_{l_{io}} = \frac{g\,(l_{io})^3\beta\,((\omega_i T_{i\infty}+\omega_o T_{o\infty})-T_{so})}{\mu^2/\rho^2}, \quad \mathrm{Pr} = \frac{\mu_{air}\,cp_{air}}{k_{air}} \tag{53}$$

where $k(W/mK)$ is the thermal conductivity, $Pr(-)$ is Prandtl number, $Ra(-)$ is Rayleigh number,$h(W/m^2K)$ is the convective heat transfer coefficient, $Gr(-)$ is Grashoff number, $l(m)$ is the length or dimension of the bath, (m/s^2) is the gravitational constant, and the thermophysical properties of the fluids found in Eqs. (48) - (53) are defined by mathematical correlation in Table. 1 [14, 16, 17].

3 Discussion and results

The presentation of results and subsequent discussion of the results is carefully articulated in this section.

3.1 The input data

Table 1: Thermal properties of the working fluids (air and water) at the fluid temperature

S♯	Parameter	Unit	Equation	
			Air	Water
1.	Temperature coefficient,β	$\left(\frac{1}{K}\right)$	$\frac{1}{T_{o\infty}}$(or$\frac{1}{T_{i\infty}}$)	$\frac{1}{T_{o\infty}}$
2.	Density,ρ	$\frac{kg}{m^3}$	$\rho = 2.1313 - 0.003T_{o\infty}$	$\rho = 754.3079871 + 1.8813$ 2843$\mathrm{T_{i\infty}} - 0.0035831\mathrm{T}^2_{i\infty}$
3.	Viscosity,μ	$\frac{kg}{m\,s}$	$\mu = 1.03\times10^{-6}+7\times10^{-8}T_{o\infty}$ $-4\times10^{-11}T^2_{o\infty}$	$\mu = 146039867076.91\,T_{i\infty}^{-5.74}$
4.	Heat capacity, cp	J/kgK; KJ/kgK^*	$cp = 1031.31 - 0.2047\,T_{o\infty}$ $+0.00042\,T^2_{o\infty}$	$cp^* = 5.476 - 0.008178$ $T_{i\infty} + 0.000013T^2_{i\infty}$
5.	Thermal conductivity, k	$\frac{W}{m\,K}$	$\mathrm{k} = 0.0121\mathrm{e}^{(0.0025\,T_{o\infty})}$	$\mathrm{k} = 0.0223\,T_{i\infty}^{0.5802}$
6.	Air speed, u	$\frac{m}{s}$	1.4	

Table. 1 is the summary of the thermal properties of the heat transfer fluids employed in the experimentation and in computing the numerical values of the working fluids properties. The characteristic roots or eigenvalue of the transcendental equations (Eqs. (36) and (37) commensurate to the boundary conditions in Fig. 2 have been solved by Ozisik [1] for the first six roots. However, the results are made handy by transforming them into regression models in Table. 2 for the wide range of ratio of convective heat transfer coefficient to the thermal conductivity of the material (mild steel sheet). The regression coefficient, R^2 in Table. 2 portrays that there is strong correlation among the separation constants since R^2 is virtually unity for the models.

3.2 Results

Table. 2 presents the experimental results (cooling data) obtained from the operation of the ITR.

Table 2: The separation constants of transcendental equations (Eqs. (36) and (37))

S♯	Root of transcendental equation	Regression coefficient, R^2
1.	$\lambda_6 \approx 15.705980232456 + 0.069430947598\ (h/k)$ $-0.001647564096\ (h/k)^2 + 0.000021069658\ (h/k)^3$ $-0.000000135856\,(h/k)^4 + 0.000000000345(h/k)^5$	1.0000
2.	$\lambda_5 \approx -51.833 + 6.9285\,\lambda_6 - 0.1801\,\lambda_6^2$	1.0000
3.	$\lambda_4 \approx -123.21 + 15.253\,\lambda_6 - 0.4335\,\lambda_6^2$	1.0000
4.	$\lambda_3 \approx -223.16 + 27.086\,\lambda_6 - 0.7944\,\lambda_6^2$	0.9978
5.	$\lambda_2 \approx Exp\left(-26.833 + 27.259\,\ln(\lambda_3) - 6.5473\,(\ln(\lambda_3))^2\right)\ ; \lambda_3 > 0$	0.9986
6.	$\lambda_1 \approx Exp\left[\begin{array}{c} -0.1546 + 0.3514\ \ln(h/k)\ - 0.00496\ (\ln\ (h/k))^2 - 0.0042\ (\ln((h/k)))^3 \\ +0.0006\ (\ln(h/k))^4 + 0.00008\,(\ln(h/k))^5 \end{array}\right]$; $h/k > 0$.	1.0000

3.3 Discussion

Pertinently, Fig. 4 and Fig. 5 reveal the mathematical functions governing the real behaviour of the ITR; the excess temperature for the various mid-fluid temperatures and fixed steady state fin parameter; and the excess temperature for variable steady state fin parameters and fixed mid-fluid temperature, respectively. The mathematical functions are made up of Euler exponential functions associated to the homogeneous solution of the inherent boundary value problem (BVP) and linear function emanating from the nonhomogeneous solution of the differential or mechanistic equations of BVP.

Similarly, both mathematical functions characterized the solution of initial value problem (IVP).

Significantly, a low steady state fin parameter indicates that the material or surface being tested has high thermal conductivity. Conversely, a high steady state fin parameter which confirms that the tested surface or material has low thermal conductivity. The effect of steady state fin parameter on the excess temperature becomes pronounced at low value of the steady state fin parameter whereas the linear term dominates the behaviour of the model solution (an axial variation of excess temperature along the cylindrical surface) at a high value of the steady state fin parameter.

In like manner, Fig. 5 presents the simulated results of the excess temperature at specified mid-fluid temperature and variable steady state fin parameters. Uniquely, the plot is useful for establishing the relationship between the mid-fluid temperature and excess surface temperature as shown in Fig. 6. One of the benefits of the simulation is the revelation of the mid-fluid temperature between the outer and inner cylindrical test surfaces for a known practical excess surface temperature, which is experimentally awkward to measure sequel to configuration of the ITR. For the known mid-fluid temperature in Fig. 7, the practical steady state fin parameter was fished out among the multiple values of the steady state fin parameter. Unequivocally, Fig. 7 shows that the magnitude of true steady state fin parameter is 12 m^{-1} for the mild steel cylindrical test surface.

Thus, thermal conductivity of the cylindrical test surface is computed in Table. 4 as 51.929 $Wm^{-1}K^{-1}$ based on the definition of steady state fin parameter for a mild steel (0.1%C). The result (51.929 $Wm^{-1}K^{-1}$) is in good agreement with the literature value of 54 $Wm^{-1}K^{-1}$ [4]. This substantiates the fact that analytical techniques is a reliable way to unveil the thermal conductivity of material amidst other established analytical methods (inverse problem method, etc) according to Kuye et al. [8] and Ozisik [1].

Fig. 9 a displays the practical excess surface temperature variation with time. This curve simply represents the rate of cooling of the heated outer cylindrical surface. Essentially, plotting the dimensionless excess temperature along the cylindrical surface of the ITR against time in Fig. 9b yields Newtons cooling rate constant (0.0005222 s^{-1}) which signifies the rate of thermal dissipation through the outer cylindrical surface of the ITR to the surroundings. A high and low cooling rate constant indicates that there is rapid and retarded rate of heat transfer to the surrounding air, respectively.

Fig. 10 gives the thermal diffusivity of the outer cylindrical surface as 0.0000036883 (m^2/s). This result compares favourably with the literature established result (0.00000367 m^2/s) according to Kochanowski et al. [7]. This strong agreement further buttresses the fact that analytical approach for determining thermophysical

Table 3: Measured temperature from the test surface of ITR and its surrounding (° C)

Time, t (min)	Interior bath temp (° C)	Ambient temp (° C)	Spatial distribution of temperature along the cylindrical surface,$x_o(m)$						
			0.00	0.05	0.10	0.20	0.30	0.79	0.96
0	138	28	88	65	51	40	36	29	29
2	127	28	84	63	51	40	36	29	29
4	116	28	80	62	50	40	36	29	29
6	108	28	75	59	49	40	36	30	30
8	100	28	71	57	48	39	36	30	30
10	93	28	67	55	47	39	36	30	30
12	87	28	64	53	45	38	35	30	30
14	82	28	61	52	44	38	35	30	30
16	77	28	58	50	43	37	35	30	30
18	72	28	55	48	42	36	34	30	30
20	69	28	53	46	41	36	34	30	30
22	65	28	51	45	40	35	33	30	30
24	62	28	50	44	39	35	33	30	30
26	59	28	48	43	38	34	33	30	30
28	57	28	47	42	37	34	32	30	30
30	55	28	46	41	37	33	32	30	30
32	53	28	44	40	36	33	32	30	30
34	51	28	43	39	35	32	31	30	30
36	49	28	42	38	35	32	31	29	29
38	48	28	41	38	34	32	31	29	29
40	46	28	40	37	34	32	31	29	29
42	45	28	39	36	33	31	30	29	29
44	44	28	38	36	33	31	30	29	29
46	42	28	38	35	32	31	30	29	29
48	41	28	37	35	32	31	30	29	29
50	40	28	37	34	32	30	30	29	29
52	40	28	36	34	31	30	30	29	29
54	39	28	36	34	31	30	29	29	29
56	38	28	35	33	31	30	29	29	29
58	38	28	35	33	31	29	29	29	29
60	37	28	34	33	30	29	29	29	29
62	36	28	34	32	30	29	29	29	29
64	36	28	34	32	30	29	29	29	29
66	35	28	33	32	30	29	29	29	29
68	35	28	33	32	30	29	29	29	29
70	34	28	33	31	30	29	29	29	29
72	34	28	32	31	29	29	29	29	29
74	34	28	32	31	29	29	29	29	29
76	33	28	32	31	29	29	29	29	29
78	33	28	32	31	29	29	29	29	29
80	33	28	32	31	29	29	29	29	29
82	32	28	32	31	29	29	29	29	29
84	32	28	31	30	29	29	29	29	29
86	32	28	31	30	29	29	29	29	29
88	32	28	31	30	29	29	29	29	29
90	32	28	31	30	29	29	29	29	29
92	31	28	31	30	29	29	29	29	29
94	31	28	31	30	29	29	29	29	29
96	31	28	31	30	29	29	29	29	29
98	31	28	31	30	29	29	29	29	29
100	31	28	31	30	29	29	29	29	29
102	30	28	30	30	29	29	29	29	29
...	...	...	...	...	...	...	...	...	...
140	28	28	28	28	28	28	28	28	28

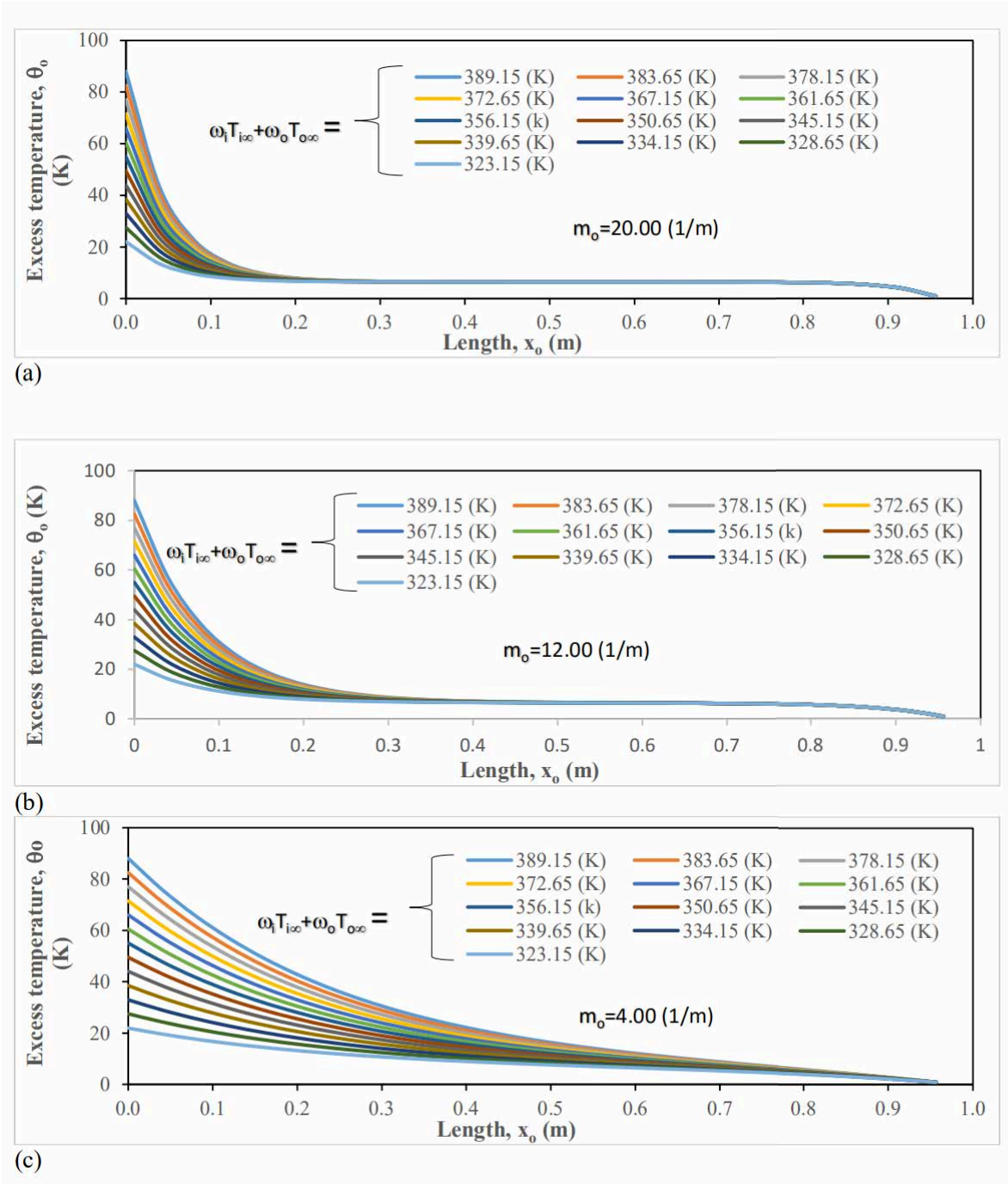

Fig. 4: Excess temperature distribution for various mid-fluid temperature ($\omega_i T_{i\infty} + \omega_0 T_{0\infty}$) on the outer hollow cylindrical surface

properties of materials should be considered premium in discovering the thermal properties of materials. Fig. 8 and Fig. 11 represent the validation of experimental and simulated data. This implies that the mechanistic or differential models were well derived from the control volume approach. A mere physical inspection of Fig. 8 and Fig. 11 without embarking on relative error analysis shows that the simulated data validated well with the experimental result which guarantees the authenticity of the thermophysical properties derived from modelling and simulation of the ITR.

Figs. 12- 14 display the distributed excess temperature curves on the outer cylindrical surface for the different values of thermal distribution coefficients. The distributed excess temperature measured is juxtaposed with the simulated ones for various conditions ($\theta_o(0,0) = \theta_{bo0}, \theta_o(0,\infty) = 0, \theta_o(1,0) = 0$ and $\theta_o(1,\infty) = 0$

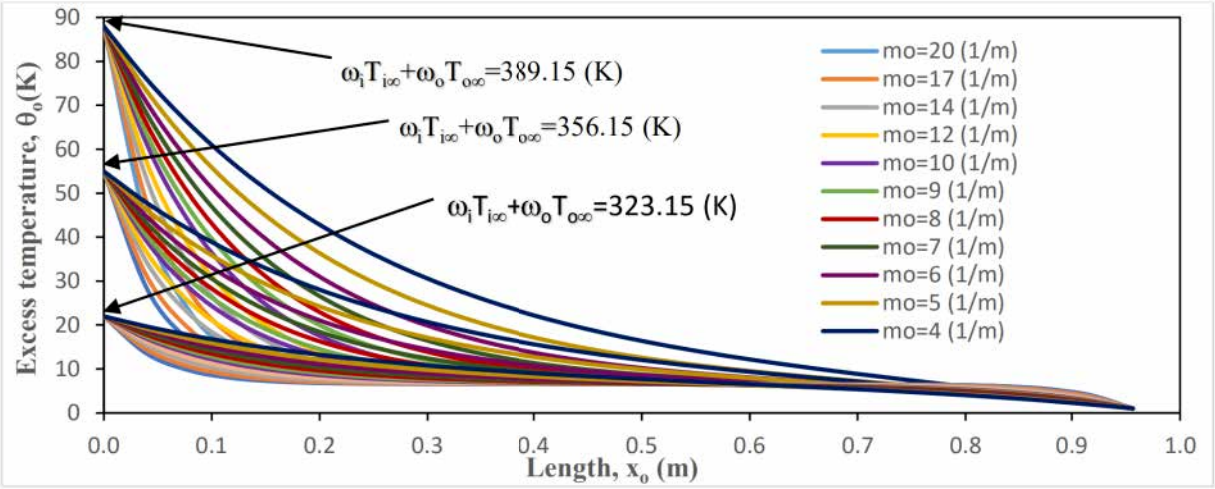

Fig. 5: Excess temperature distribution for various mid-fluid temperature (Excess temperature distribution for the various fin parameters (m_o) along the outer cylindrical surface.

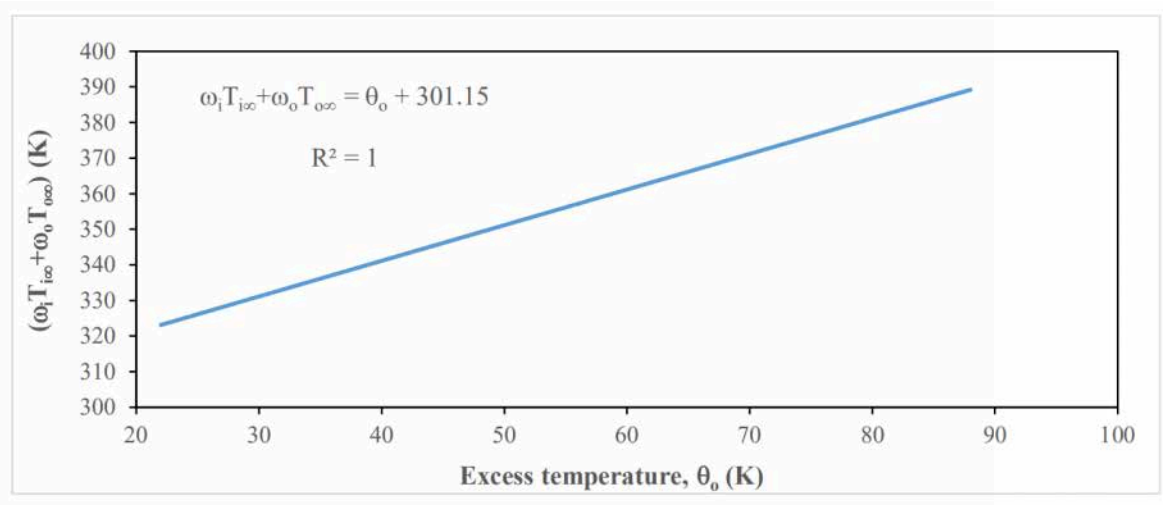

Fig. 6: Variation of mid-fluid temperature ($\omega_i T_{i\infty} + \omega_0 T_{0\infty}$) with the excess temperature on the outer cylindrical surface

Table 4: Computed thermal conductivity of the cylindrical surface (a mild steel; 0.1%C)

$h_{oo}@T_{o\infty}$	$h_{oi}@\omega_i T_{i\infty} + \omega_0 T_{0\infty}$	P_{oo}	P_{oi}	A_{co}	m_0	$k = \frac{h_{oo}P_{oo}+h_{oi}P_{oi}}{m_o^2 A_{co}}$
(W/m^2K)	(W/m^2K)	(m)	(m)	(m^2)	$(1/m)$	(W/mK)
12.329634	2.285053	0.3345257	0.32208	0.00065	12.0	51.929

). The distribution coefficients (A_o and B_o) were established by applying the various conditions and solving the quadruple equations simultaneously.

Moreover, Figs. 12- 14 indicate that there is a good agreement between the measured and simulated excess temperature for equal magnitude of distribution coefficients. Furthermore, the present work has provided a three dimensional coordinate system (3-D) analysis of the experimental data to support the validated BVP and IVP curves in Figs. 4- 8 and Figs. 9- 11, respectively.

Also, the excess temperature in the inner cylindrical surface was not simulated due to the difficulty in passing the probes into the surface. Generally, the agreement between the measured and simulated results for 2-D and 3-D plots supports the fact that the thermophysical properties obtained by the state of the art are reliable and compared to the well-known results in the literature.

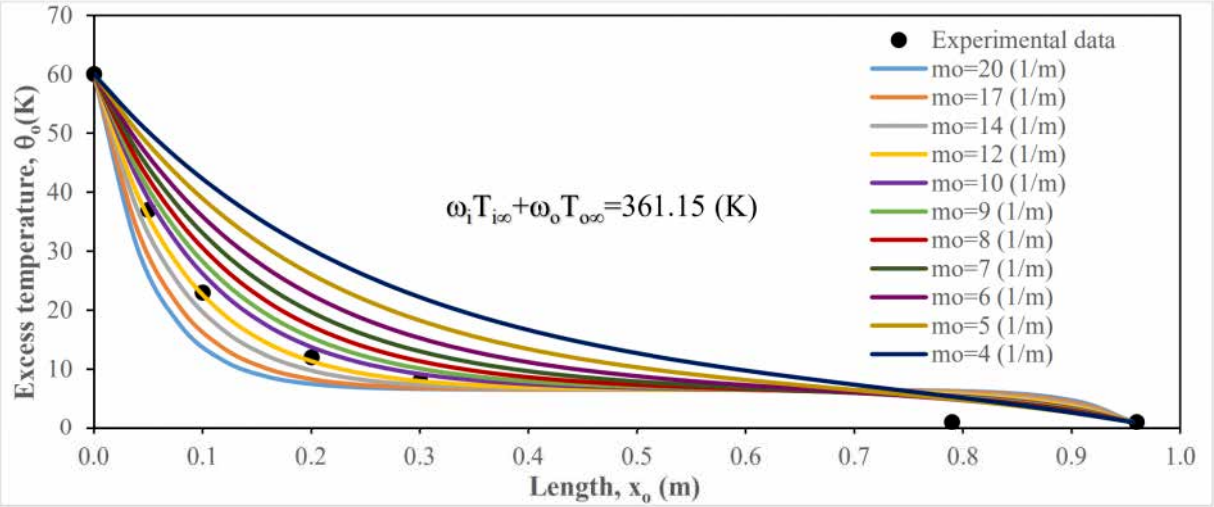

Fig. 7: Determination of practical fin parameter, $m_o(1/m)$ for known mid-fluid temperature, $(\omega_i T_{i\infty} + \omega_0 T_{0\infty})$ and excess temperature, $\theta_o(K)$ for the outer cylindrical surface

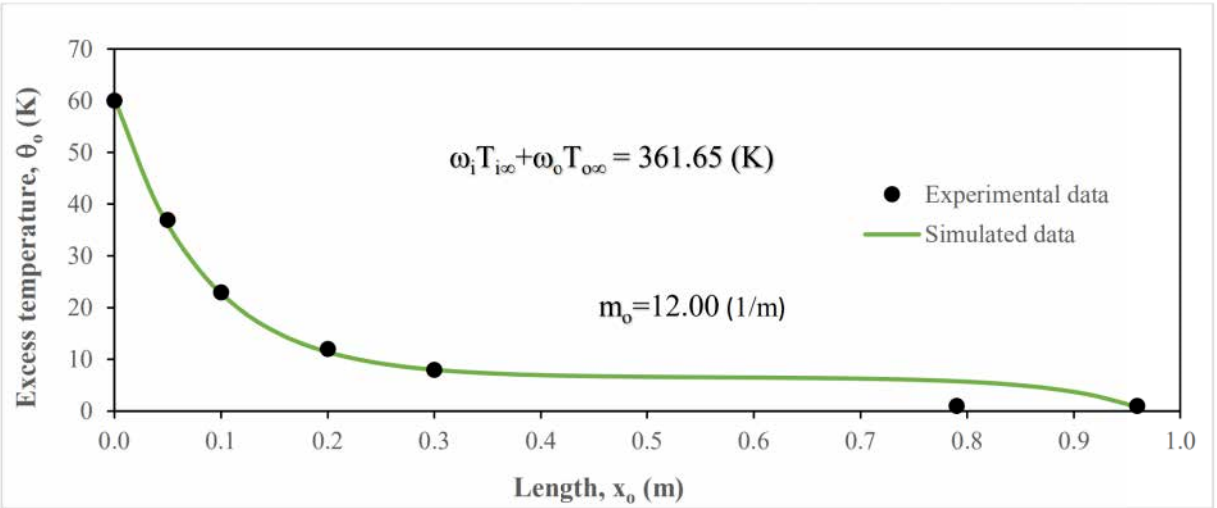

Fig. 8: Validation of excess temperature, $\theta_o(K)$ for known fin parameter, $m_o(1/m)$ and mid-fluid temperature, $(\omega_i T_{i\infty} + \omega_0 T_{0\infty})$ along the outer cylindrical surface

4 Conclusion

Modelling, simulation and experimentation on the ITR has been implemented. The linear excess temperature coefficient of the model yielded a steady state fin parameter (12 m^{-1}) for the outer cylindrical surface of the ITR. The steady state fin parameter was instrumental in determining the thermal conductivity (51.929 W/mK) of the mild steel cylindrical test surface of the ITR. The thermal diffusivity (0.0000036883 m^2/s) of the mild steel cylindrical test surface was determined from the time additive solution of the thermal model. The cooling rate (0.0005222 s^{-1}) was experimentally determined for the mild steel test suracfe of the ITR. The good agreement between the simulated and literature results (n/a; 54 W/mK; 0.00000367 m^2/s; n/a, respectively) buttresses the fact that ITR is very good for determining the thermophysical properties of materials. Also, the thermal distribution coefficients (0.333333 - 0.492277) introduced by the current work accounted for the good agreement between the simulated and experimental distributed models for the ITR. Thus, the equipment could be confidently deployed in determining the thermophysical properties of mostly fibrous agricultural wastes for potential use as insulators. Besides the industrial application, the modelling techniques, solutions and experimentation could be a repository for demonstrating modelling and simulation of thermal systems.

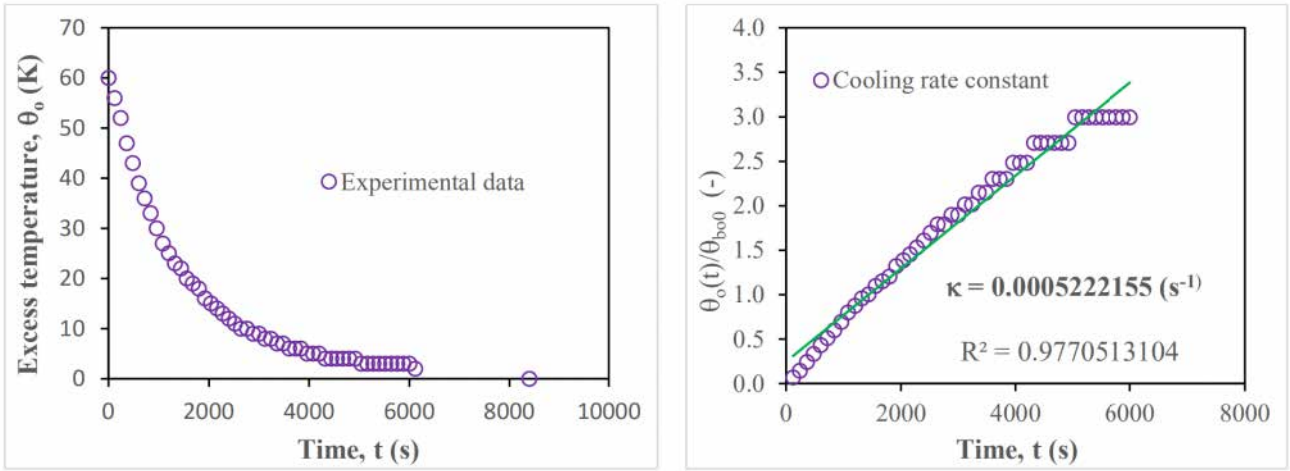

Fig. 9: Measured excess temperature history on the outer cylindrical surface

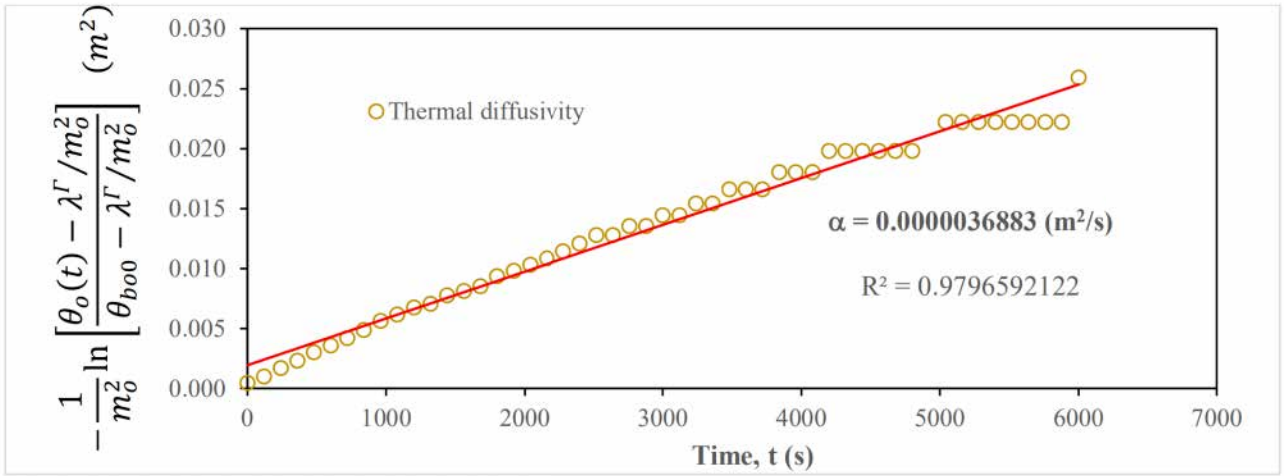

Fig. 10: Measurement of thermal diffusivity of the cylindrical surface

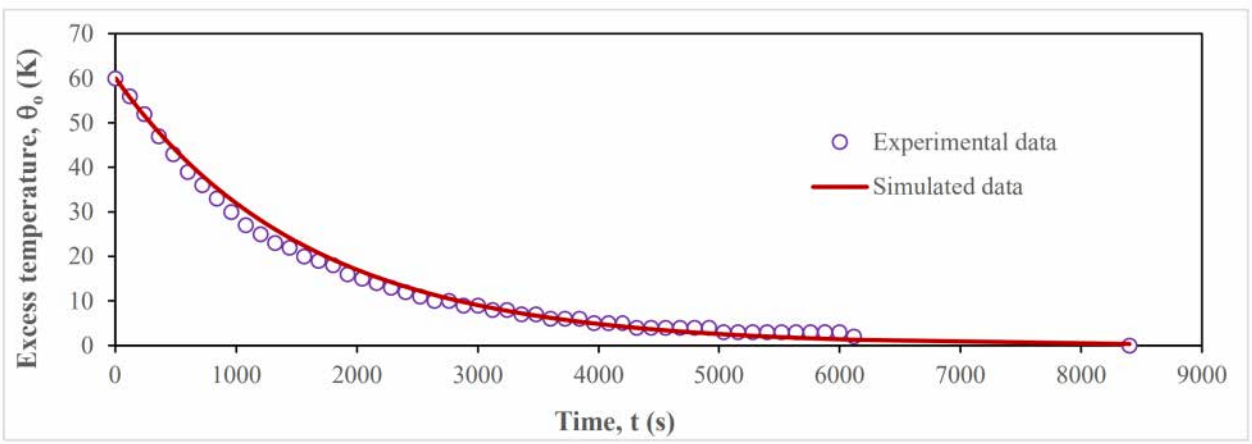

Fig. 11: Validation of excess temperature on the outer cylindrical surface

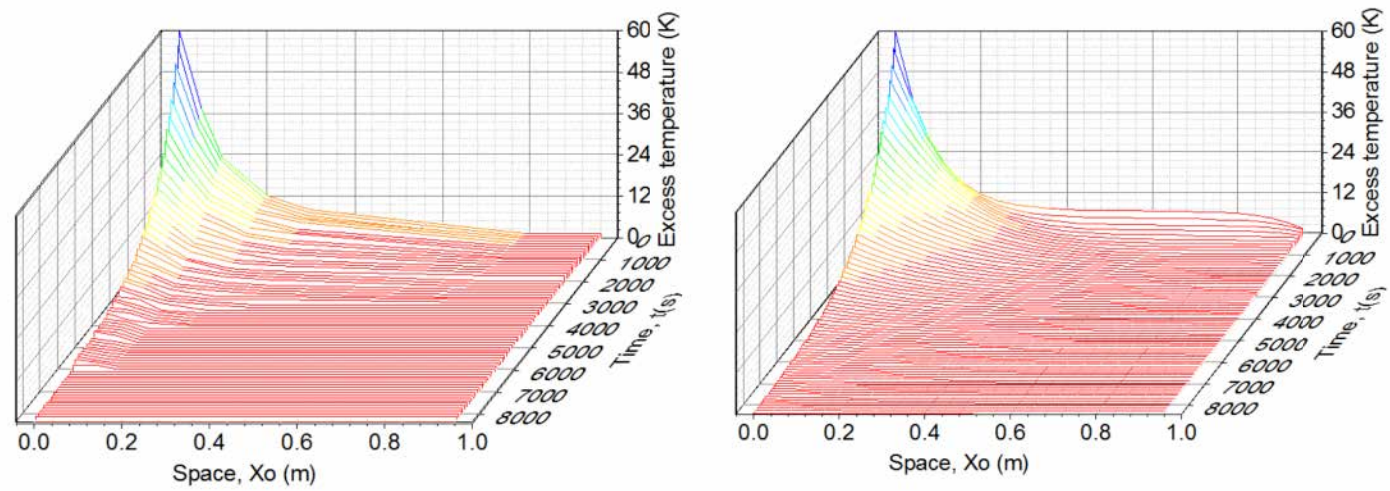

Fig. 12: Distributed excess temperature curves for $A_o = B_o = 0.492247$

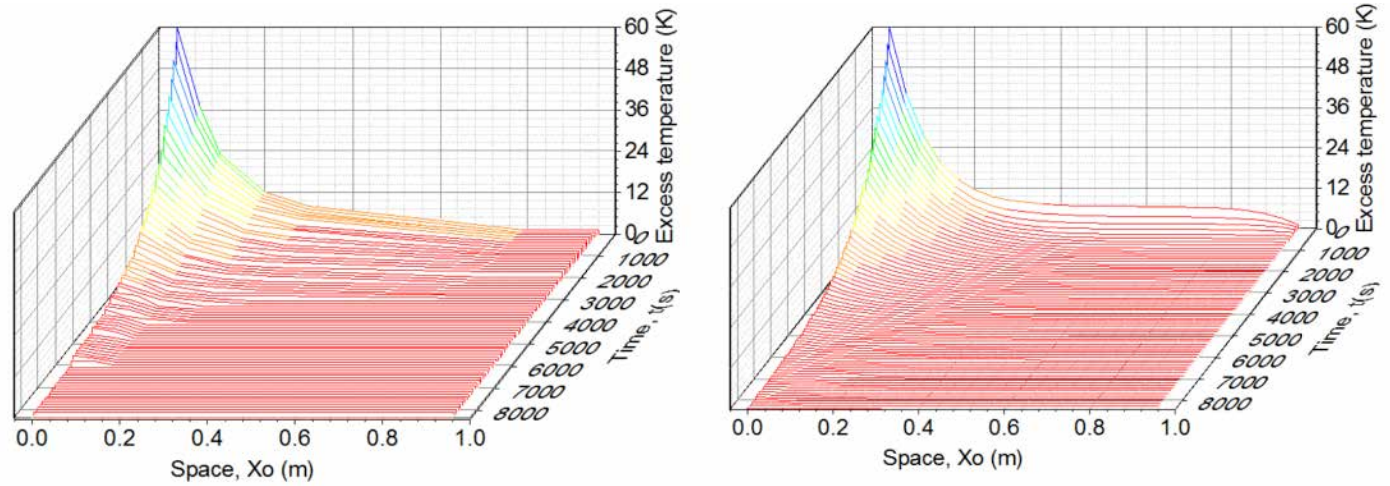

Fig. 13: Distributed excess temperature curves for $A_o = B_o = 0.39976$

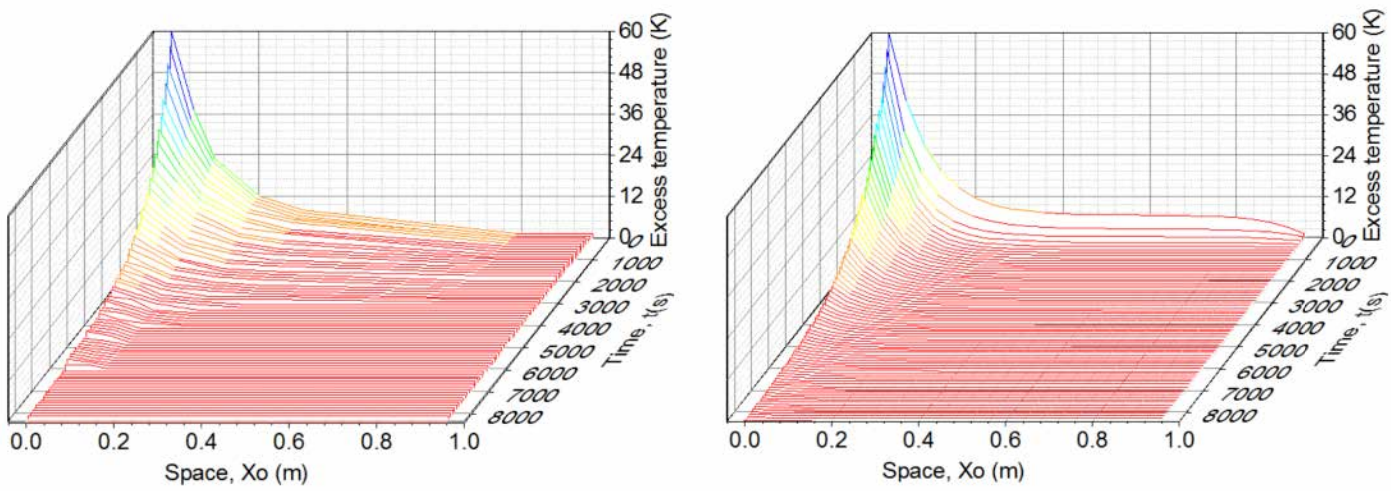

Fig. 14: Distributed excess temperature curves for$A_o = B_o = 0.333333$

Acknowledgments

The authors wish to acknowledge the Management of Kampala International University for providing the research facilities used in this work.

Funding

The authors received no direct funding for this research.

Disclosure statement

No potential conflict of interest was reported by the authors.

References

[1] M. N. Ã-zisik, M. N. Özısık, M. N. Özışık. *Heat conduction*. John Wiley & Sons, 1993.
[2] M. Al-Nimr, A. Khadrawi, M. Hammad. A generalized thermal boundary condition for the hyperbolic heat conduction model. *Heat and Mass Transfer*, 2002, **39**(1): 69–79.
[3] A. Creosteanu, G. Gavrila, L. Creosteanu. Comparison between an analytical method and two numerical methods on a given electrostatic potential determination problem. **in:** *2012 15 International Symposium on Antenna Technology and Applied Electromagnetics*, IEEE, 2012, 1–6.
[4] E. Edge. Thermal properties of metals, conductivity, thermal expansion, specific heat, 2019.
[5] M. Flori, V. Puţan, L. Vîlceanu. Using the heat flow plate method for determining thermal conductivity of building materials. **in:** *IOP Conference Series: Materials Science and Engineering*, vol. 163, IOP Publishing, 2017, 012018.
[6] H. Jia, W. Xu, X. Zhao, Z. Li. Separation of variables and exact solutions to nonlinear diffusion equations with x-dependent convection and absorption. *Journal of Mathematical Analysis and Applications*, 2008, **339**(2): 982–995.
[7] K. Kochanowski, W. Oliferuk, Z. Płochocki, A. Adamowicz. Determination of thermal diffusivity of austenitic steel using pulsed infrared thermography. *Archives of Metallurgy and Materials*, 2014, **59**(3): 893–897.
[8] A. Kuye, C. Oko, S. Nnamchi. Determination of the thermal conductivity and specific heat capacity of neem seeds by inverse problem method. *Journal of Engineering Science and Technology Review*, 2010, **3**(1): 1–6.
[9] S. A. Lawal, B. I. Ugheoke. Development and performance evaluation of thermal conductivity equipment for laboratory uses. *Annals of the Faculty of Engineering Hunedoara*, 2012, **10**(2): 49.
[10] M. Li, H. Zhang, Y. Ju. Design and construction of a guarded hot plate apparatus operating down to liquid nitrogen temperature. *Review of Scientific instruments*, 2012, **83**(7): 075106.
[11] G. Marion, D. Lawson. An introduction to mathematical modelling. *Edinburgh: Bioinformatics and Statistics Scotland, University of Bristol*, 2008.
[12] R. McMasters, Z. J. Harth, R. P. Taylor, G. M. Brooke. Testing extremely small samples using the flash diffusivity method. *International Journal of Numerical Methods for Heat & Fluid Flow*, 2017, **27**(3): 551–560.
[13] S. Nnamchi, O. Nnamchi, E. Sangotayo, M. Mundu, O. Edosa. Design and fabrication of insulation testing rig. *Indian Journal of Engineering*, 2019, **16**: 60–79.
[14] S. Nnamchi, O. Sanya, K. Zaina, V. Gabriel. Development of dynamic thermal input models for simulation of photovoltaic generators. *International Journal of Ambient Energy*, 2018, 1–13.
[15] C. Oko. Mathematical modelling and operations research, 2009.
[16] C. Oko, S. Nnamchi. Energy and exergy audit of a solar grain dryer. *International Journal of Renewable Energy Technology*, 2011, **3**(1): 79–93.
[17] C. Oko, S. N. Nnamchi. Heat transfer in a low latitude flat plate solar collector. *Thermal Science*, 2012, **16**(2): 583–591.
[18] S. Olusunle, B. Ebiwonjumi, R. Medupin. Mathematical modeling: A tool for material corrosion prediction. 2011.
[19] D. Salmon. Thermal conductivity of insulations using guarded hot plates, including recent developments and sources of reference materials. *Measurement Science and Technology*, 2001, **12**(12): R89.
[20] S. Sistemas. External flow correlations (average, isothermal surface), 2008.
[21] B. Skočilasová, J. Skočilas, J. Soukup. Forced convection and heat transfer around a bounded cylinder. **in:** *MATEC Web of Conferences*, vol. 157, EDP Sciences, 2018, 02045.
[22] G. Wang, Z. Wang, Q. Yu, Y. Song, Y. Wu, W. Cheng. Heat transfer experiment and simulation of the verification facility for high power rotating tritium target system. *Journal of Fusion Energy*, 2015, **34**(6): 1252–1256.

[23] A. White, M. Tolman, H. D. Thames, H. R. Withers, K. A. Mason, M. K. Transtrum. The limitations of model-based experimental design and parameter estimation in sloppy systems. *PLoS computational biology*, 2016, **12**(12): e1005227.